Human Molecular Genetics, 2013, Vol. 22, No. 7 ***1358–1372***
doi:10.1093/hmg/dds546
Advance Access published on January 2, 2013

Variable expressivity of ciliopathy neurological phenotypes that encompass Meckel–Gruber syndrome and Joubert syndrome is caused by complex de-regulated ciliogenesis, Shh and Wnt signalling defects

Zakia A. Abdelhamed[1,2], Gabrielle Wheway[1], Katarzyna Szymanska[1], Subaashini Natarajan[1], Carmel Toomes[1], Chris Inglehearn[1] and Colin A. Johnson[1,*]

[1]Ciliopathy Research Group, Section of Ophthalmology and Neurosciences, Leeds Institute of Molecular Medicine, University of Leeds, Leeds LS9 7TF, UK and [2]Department of Anatomy & Embryology, Faculty of Medicine, Al-Azhar University, Cairo, Egypt

Received October 31, 2012; Revised and Accepted December 20, 2012

The ciliopathies are a group of heterogeneous diseases with considerable variations in phenotype for allelic conditions such as Meckel–Gruber syndrome (MKS) and Joubert syndrome (JBTS) even at the inter-individual level within families. In humans, mutations in *TMEM67* (also known as *MKS3*) cause both MKS and JBTS, with *TMEM67* encoding the orphan receptor meckelin (TMEM67) that localizes to the ciliary transition zone. We now describe the *Tmem67*$^{tm1(Dgen/H)}$ knockout mouse model that recapitulates the brain phenotypic variability of these human ciliopathies, with categorization of *Tmem67* mutant animals into two phenotypic groups. An MKS-like incipient congenic group (F6 to F10) manifested very variable neurological features (including exencephaly, and frontal/occipital encephalocele) that were associated with the loss of primary cilia, diminished Shh signalling and dorsalization of the caudal neural tube. The 'MKS-like' group also had high de-regulated canonical Wnt/β-catenin signalling associated with hyper-activated Dishevelled-1 (Dvl-1) localized to the basal body. Conversely, a second fully congenic group ($F > 10$) had less variable features pathognomonic for JBTS (including cerebellar hypoplasia), and retention of abnormal bulbous cilia associated with mild neural tube ventralization. The 'JBTS-like' group had de-regulated low levels of canonical Wnt signalling associated with the loss of Dvl-1 localization to the basal body. Our results suggest that modifier alleles partially determine the variation between MKS and JBTS, implicating the interaction between Dvl-1 and meckelin, or other components of the ciliary transition zone. The *Tmem67*$^{tm1(Dgen/H)}$ line is unique in modelling the variable expressivity of phenotypes in these two ciliopathies.

INTRODUCTION

Meckel–Gruber syndrome (MKS) is a lethal ciliopathy disorder that is usually diagnosed upon detection of a triad of manifestations that include renal cystic kidney dysplasia, polydactyly and neurodevelopment anomalies (1,2). The central nervous system (CNS) defects commonly observed in MKS include occipital encephalocele, rhombic roof dysgenesis and prosencephalon dysgenesis. The latter may include olfactory bulb dysgenesis, optic nerve hypoplasia, agenesis of the corpus callosum or total holoprosencephaly. These defects are thought to be caused by an underlying defect in ventral induction of the developing CNS by the prochordal mesoderm (3). Other occasional CNS features of MKS include

*To whom correspondence should be addressed at: Department of Ophthalmology and Neurosciences, Leeds Institute of Molecular Medicine, Wellcome Trust Brenner Building, St James's University Hospital, Leeds LS9 7TF, UK. Tel: +44 1133438443; Fax: +44 1133438603; Email: c.johnson@leeds.ac.uk

microcephaly, cerebellar hypoplasia or total anencephaly (4). The human condition is both genetically and phenotypically heterogenous, and displays marked phenotypic and genetic overlap with the allelic neurodevelopmental disorder Joubert syndrome (JBTS) (5). JBTS neurodevelopmental phenotypes involve cerebellar vermis hypoplasia or aplasia, a deep interpeduncular fossa and narrowing of the midbrain tegmentum. Collectively, these features are visualized on axial MRI with the characteristic 'molar tooth sign' (MTS) that is pathognomonic for this condition (6).

MKS and JBTS are ciliopathies (5,7–9), caused by mutations in genes encoding proteins that are components of the primary cilium and basal body. Primary cilia are microtubule-based organelles that sense and transduce extracellular signals on many cell types during the G_1/G_0 phase of the cell cycle (10–12), and it is now well established that cilia mediate key pathways of embryonic development such as Wnt and Shh signalling (13,14). The role of cilia in regulating canonical (β-catenin-mediated) Wnt remains unclear, with some studies showing that cilia act as a negative regulator of canonical Wnt signalling, suggesting that the loss of cilia leads to activation of the canonical Wnt signalling. For example, high levels of cytoplasmic and nuclear β-catenin were present in postnatal cystic kidneys (15) and pancreas (16) of animal models with mutations in *Kif3a* and IFT genes, respectively. These findings suggest that β-catenin degradation is a process that requires cilia and/or basal bodies. In addition, members of the destruction complex, Gsk-3β (17) and APC (18), are localized to cilia, and primary cilia restrict the activity of canonical Wnt signalling pathway in mouse embryo, primary fibroblast and embryonic stem cells. Recently, Lancaster *et al.* (19) confirmed that primary cilia constrain canonical Wnt signalling through β-catenin cytosolic stabilization, whereas cells with multiple cilia have suppressed canonical Wnt/β-catenin signalling. In contrast, studies in other ciliopathy models with cilia defects demonstrate that the Wnt pathway was not disrupted in zebrafish (20) or mouse embryos (21). This may suggest a context-dependant regulation of canonical Wnt signalling by primary cilia.

To further elucidate the role of Shh and Wnt signalling in the severe human ciliopathies such as MKS with occipital encephalocele and JBTS, and the possible molecular basis for the variability of the neurodevelopmental anomalies, we studied embryonic neurodevelopmental, cilia and Wnt/β-catenin signalling phenotypes in the *Tmem67*$^{tm1(Dgen/H)}$ knockout mouse line (22). *Tmem67* encodes Tmem67 (transmembrane protein 67 or meckelin), a 995 amino-acid transmembrane protein (Supplementary Material, Fig. S1A), with structural similarity to Frizzled receptors (23). Meckelin/TMEM67 contains an extracellular N-terminal domain with a highly conserved cysteine-rich repeat domain (CRD), a predicted β-pleated sheet region and seven predicted transmembrane regions (Supplementary Material, Fig. S1A). The knock-out line recapitulated complex and variable features of both MKS-like and JBTS-like phenotypes: one group of incipient congenic animals developed frontal/occipital meningo/encephalocelle-like anomalies (Fig. 1), whereas a second group of fully congenic animals had a less variable range of features pathognomonic of JBTS (Fig. 2).

RESULTS

Tmem67$^{-/-}$ mutants display typical pathological features of Meckel–Gruber and Joubert syndromess

To study the mechanism of MKS and JBTS disease pathogenesis, we investigated the detailed neuroanatomical phenotypes of the *Tmem67*$^{tm1(Dgen/H)}$ targeted knockout mouse model. Reverse transcription (RT)–PCR analysis confirmed that targeted *β-Gal-neo* cassette insertion into *Tmem67* abolished transcription of *Tmem67* in *Tmem67*$^{-/-}$ embryos (Supplementary Material, Fig. S1B). Protein expression was assessed by immunoblotting cell lysates with a rabbit polyclonal antibody ('Nt Ab') raised against the TMEM67 CRD domain, which confirmed the absence of TMEM67 in *Tmem67*$^{-/-}$ embryos (Supplementary Material, Fig. S1C). *Tmem67*$^{-/-}$ mutants died by the first or second postnatal day (P0–P1) and recapitulated the histological features of MKS and JBTS (24), including multicystic renal dysplasia and embryonic developmental defects of the biliary tree (data not shown). Renal cystic dysplasia was an obligate feature for all animals analyzed at all developmental stages, manifesting by embryonic day 15.5 (E15.5) in both the 'MKS-like' and 'JBTS-like' groups. Neither pre-axial nor post-axial polydactyly was observed in any mutant embryo or pup, although syndactyly was noted in one embryo (data not shown).

An MKS-like phenotype manifested in 35% of E11.5 embryos ($n = 6/17$; Table 1), of which $n = 1/6$ had an occipital meningocele that was detected externally as a bulge in the occipital area (Fig. 1A). Midbrain-hind brain exencephaly, with a failure of fusion of the neural folds, was noted in some E11.5 embryos ($n = 4/17$; Table 1, Fig. 1B), as was an anterior neuropore closure defect ($n = 4/17$; Table 1, Fig. 1C). At later developmental stages (from E13.5), frontal encephalocele had a variable degree of severity from a very mild defect (slight protrusion in the frontal area) to a gross encephalocele/meningocele-like anomaly seen in either a median or paramedian position ($n = 5/19$) (Fig. 1D and E). In the former type, the encephalocele protruded midline of the frontal area, while for the latter it protruded from one of the hemispheres (Fig. 1D). Prosencephalon dysgenesis was a consistent finding for all E11.5 embryos that could be diagnosed with MKS-like features ($n = 7/7$; Table 1). At later developmental stages, this manifested as semi-lobar holoprosencephaly in which the two lateral ventricles were fused with an absence of some midline structures such as the anterior commissar and variable degrees of corpus callosum dysgenesis (Fig. 1F). The 'MKS-like' group of animals also had enlargement of the hippocampus (25–27) and basal ganglia (28) (Fig. 1F), both suggestive of an up-regulation of canonical (β-catenin-mediated) Wnt signalling. IHC staining of encephalocele tissue demonstrated an increased level of activated β-catenin (Fig. 1G), and a mixed population of post-mitotic and progenitor neurons as indicated by the neuronal differentiation marker Tuj1 (Fig. 1G).

The second, JBTS-like phenotype manifested in 58% of later stage *Tmem67*$^{-/-}$ embryos and pups ($n = 11/19$; Table 2). The JBTS group of *Tmem67*$^{-/-}$ mutant embryos had no overt neural tube defect, but all animals had a reduced anteroposterior axis of the developing forebrain (Table 2), in addition to a small

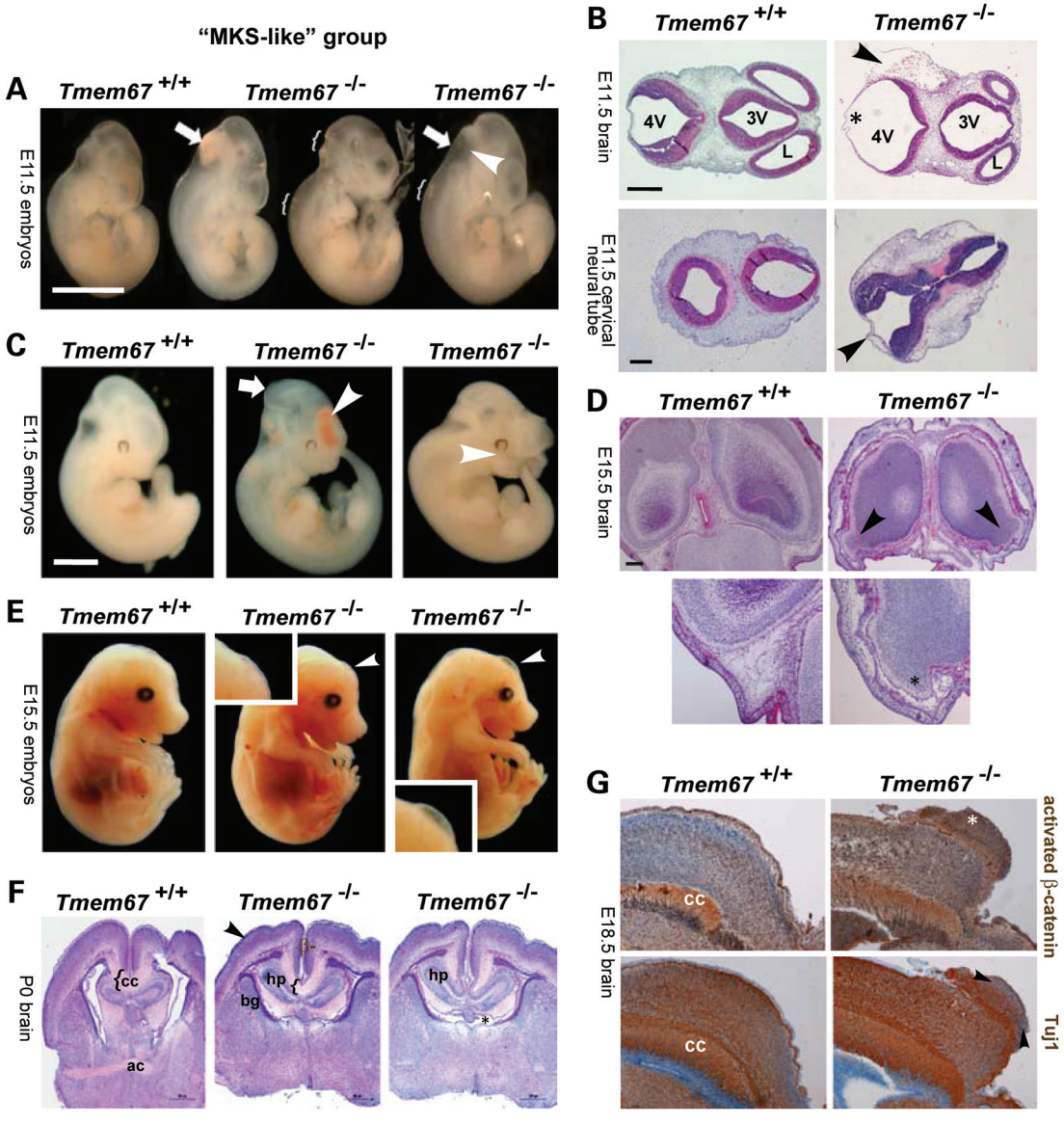

Figure 1. MKS-like neurodevelopmental defects in *Tmem67*$^{-/-}$ mouse embryos: (**A**) whole embryo images showing phenotypic variability in *Tmem67*$^{-/-}$ compared with *Tmem67*$^{+/+}$ congenic littermates at embryonic age E11.5. Indicated are occipital meningocele (arrows), cranial neural tube defects affecting midbrain and hindbrain regions, localized areas of spinal neural tube defects (braces) and cystic dilated fourth ventricle and expanded roof plate (arrowhead). Scale bar = 5 mm. (**B**) H&E stained horizontal brain sections of E11.5 *Tmem67*$^{-/-}$ mutants. Top panels: meningocele with a prominent defect in the head mesoderm (arrowhead) surrounding the hindbrain, dilated fourth ventricle (4V) and roof plate malformation (asterisk). Bottom panel: failure of neural groove closure at the level of the mesencephalon (arrowhead). Scale bars = 1 mm. (**C**) Whole embryo images of E11.5 congenic littermates showing anterior neuropore closure defect (forebrain haemorrhage) (middle panel, arrowhead), and midbrain exencephaly (middle panel, arrow) and forebrain exencephaly (right panel, arrowhead) in *Tmem67*$^{-/-}$. (**D**) H&E sections of occipital encephalocele (arrowheads and asterisk) in E15.5 *Tmem67*$^{-/-}$ embryos. Scale bar = 0.1 mm. (**E**) Frontal encephalocele in E15.5 *Tmem67*$^{-/-}$ embryos (arrowheads, detail shown in insets). (**F**) Semi-lobar holoprosencephaly in P0 *Tmem67*$^{-/-}$ pups showing fusion of the two lateral ventricles (asterisk), absence of the anterior commissar (ac) and corpus callosum (cc) dysgenesis (indicated by braces), enlarged hippocampus (hp) and basal ganglia (bg), reduced cortical thickness and frontal encephalocele (arrowhead). (**G**) E18.5 *Tmem67*$^{-/-}$ brain sectioned and stained for activated β-catenin and the neuronal differentiation marker Tuj1. Arrowheads indicate a region of neuronal progenitors in a frontal encephalocele (asterisk). Scale bar = 1 mm.

hindbrain region, microcephaly or other overt facial dysmorphologies (Fig. 2A). Some embryos in the JBTS group of *Tmem67*$^{-/-}$ mutants had a deep interpenduncular fossa with a reduced anterioposterior axis of the midbrain tegmentum at the level of the isthmus (Fig. 2A), accompanied by cerebellar vermis hypoplasia or aplasia (Fig. 2B and C). These features comprise the MTS that is pathognomonic for JBTS in humans. Dilatation of the fourth ventricle was not noted in this group, but complex posterior fossa defects (Fig. 2D) and features compatible with the Dandy–Walker malformation (Supplementary Material, Fig. S2A) were seen, all of which are reported in human patients either in combination with the diagnostic MTS or as separate anomalies in the so-called 'Joubert syndrome mimicry' group (29).

In general, incipient congenic embryos (F6–F10 filial generations on the C57BL/6J background) manifested a very

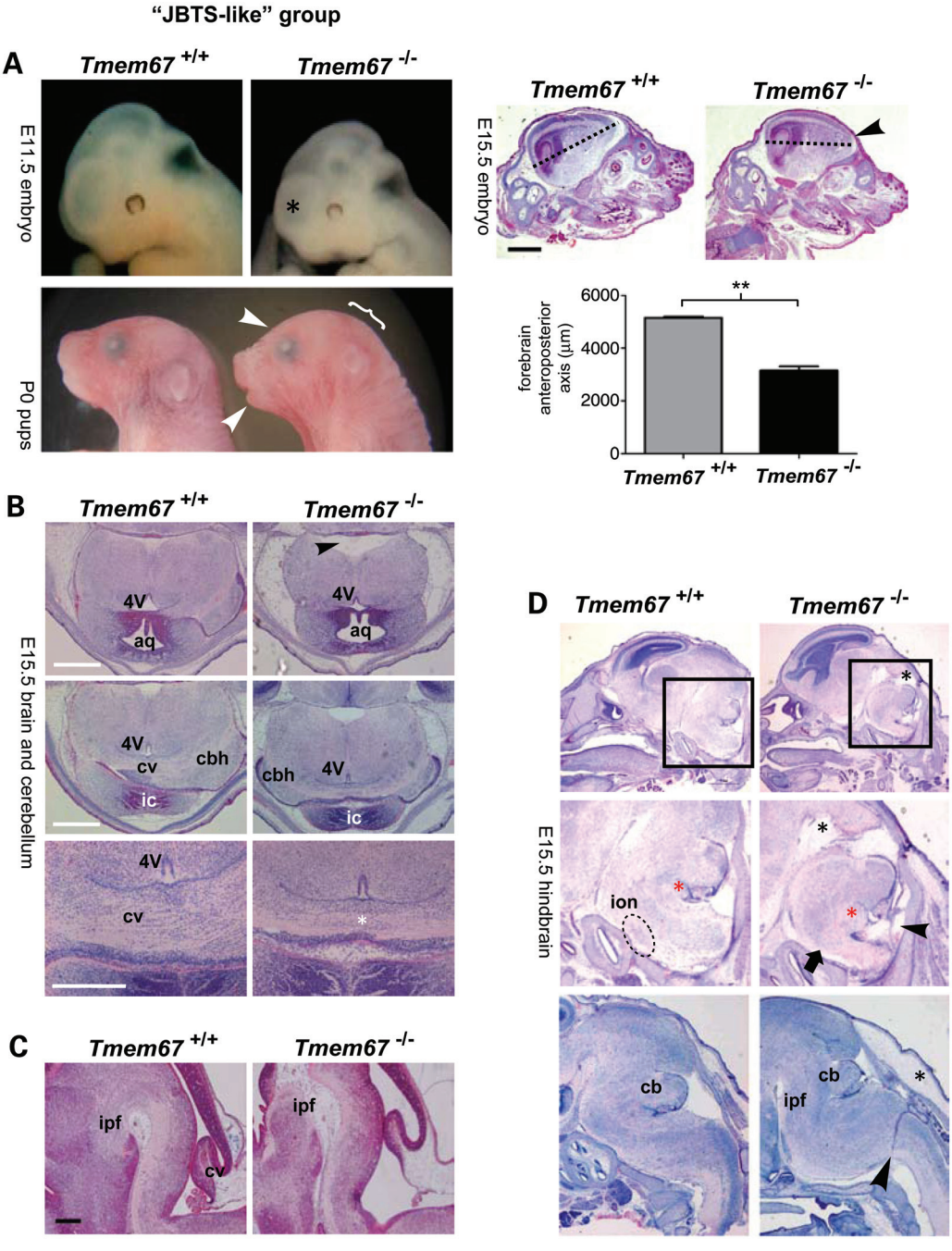

Figure 2. JBTS-like posterior fossa and cerebellar hypoplasia defects in *Tmem67*$^{-/-}$ mouse embryos: (**A,** left panels) small hind brain region in E11.5 *Tmem67*$^{-/-}$ embryos and smaller forebrain (asterisk). (Middle panel) Reduced hind brain region (brace) and hypoplastic mandible (arrowhead) in P0 *Tmem67*$^{-/-}$ pups. (Right panel) Reduced anteroposterior axis (dotted lines) of the developing forebrain in E15.5 *Tmem67*$^{-/-}$ embryos, quantitated in the bar graph. Values shown are means of three independent replicates. (**B**) Horizontal brain sections of E15.5 *Tmem67*$^{-/-}$ embryos showing pathognomonic features of JBTS, including a deep interpeduncular fossa (top panel, arrowhead) and reduction in the anteroposterior axis of the midbrain, and cerebellar vermis aplasia or hypoplasia (middle and bottom panels, asterisk). (**C**) Mid-sagittal sections of *Tmem67*$^{-/-}$ E12.5 embryos showing cerebellar vermis hypoplasia. Scale bars = 50 μm. (**D**) Complex posterior fossa defects in the E15.5 *Tmem67*$^{-/-}$ embryonic hindbrain (top panel, with middle panel showing magnified insets indicated by black frames), showing marked dysplasia of the caudal medulla, absence of the inferior olive nucleus (dashed oval, arrow in mutant), deep abnormal interpeduncular fossa (black asterisk), abnormally dilated cisterna magna and septa (arrowhead) and an enlarged and protruding locus coeruleus (red asterisk). (Lower panel) Dysplastic cervico-medullary junction (arrowhead) and overlying head structure (asterisk). Scale bar = 1 mm. Abbreviations: 4V, fourth ventricle; aq, aquaduct; cb, cerebellum; cbh, cerebellar hemispheres; cv, cerebellar vermis; ic, inferior colliculus; ion, inferior olive nucleus ipf, interpenduncular fossa.

variable MKS-like phenotype, whereas fully congenic animals ($F > 10$) had the less variable JBTS-like phenotype (Table 2; $P < 0.001$, Chi-squared test). However, we also noted inter-individual variation in these phenotypes, even for *Tmem67*$^{-/-}$ mutant littermates (Supplementary Material, Fig. S2B).

Table 1. Summary of neurodevelopmental anomalies detected in *Tmem67*$^{-/-}$ mutants at the E11.5 stage of development

Phenotype(s)	*Tmem67*$^{-/-}$ mutant animals																	Total/17
	F6–F10												F>10					
	1	2	3	4	5	6	7	8	9	10	11	12	13	14	15	16	17	
Meningocele-like	✓	✓																1
MB exencephaly	✓				✓			✓			✓							4
Rh. dysgenesis	✓				✓								✓	✓				4
Expanded roof plate		✓	✓	✓	✓			✓			✓	✓			✓	✓	✓	11
Forebrain																		
Pros. dysgenesis							✓				✓	✓						3
Pros. normal but small	✓	✓	✓	✓	✓	✓		✓	✓	✓							✓	11
sNTD	✓	✓	✓	✓														4
Phenotype group	M	M	M	M	M	–	–	M	–	–	M	–	–	–	–	–	–	

In total, 17 *Tmem67*$^{-/-}$ animals at E11.5 were examined morphologically or histologically, out of 49 animals of all genotypes from 5 timed matings. Individual animals (numbered 1–17) are separated on the basis of filial generation (F6–F10, or F>10, as indicated) after back-crossing onto the C57BL/6J genetic background. The bottom row indicates if each individual animal had features compatible with MKS (M), or if a definitive diagnosis could not be made at this stage of development (–). Abbreviation: M, MKS-like phenotype group; MB, midbrain; Rh, rhombencephalon; Pros, prosencephalon; sNTD, spinal neural tube defect.

The MKS-like phenotype is associated with cilia loss and caudal neural tube dorsalization, whereas the JBTS-like phenotype is associated with aberrant cilia structure and mild neural tube ventralization

To investigate ciliary phenotypes in 'MKS-like' *Tmem67*$^{-/-}$ mutants, we stained caudal neural tube sections from E11.5 and E14.5 embryos for primary cilia and basal bodies. This revealed near total loss of cilia at the developing neuroepithelial cell layer (Fig. 3A and B), confirmed by *in vivo* SEM of the ependymal cell layer of *Tmem67*$^{-/-}$ E18.5 lateral ventricle (Fig. 3C). In contrast, the JBTS group of mutant animals retained primary cilia at the E11.5 neuroepithelial cell layer of the caudal neural tube (Fig. 3D), and both IF microscopy and SEM revealed that ependymal cells had abnormal, bulbous cilia (Fig. 3E). Furthermore, in both the MKS-like and JBTS-like disease states, the planar organization of the ependymal cell layer was disrupted (Fig. 3C and E).

Loss of cilia causes suppression of the Shh pathway, since the activation of Shh signalling requires the translocation of Smo to the primary cilia following binding of Shh ligand to the Patched receptor (30). We therefore investigated the expression of the Shh protein and dorsoventral neural tube markers in the caudal neural tube of E11.5 *Tmem67*$^{-/-}$ embryos with an MKS-like phenotype. Embryos had a variable, thinning defect of the roof plate, Shh protein expression was reduced at the mutant floor plate and notochord, and a reduced number of cells expressing the floor plate marker Foxa2 (Fig. 4A). Cells labelled with the ventral markers NKx2.1 and NKx6.1 were also reduced in number and more ventrally located in the 'MKS-like' *Tmem67*$^{-/-}$ neural tube (Fig. 4A). There was a slight increase and ventral expansion of cells labelled with the dorsal marker Pax6, but localization of Pax7 expression was unaffected (Fig. 4A). Together, these data indicated a dorsalization of the neural tube in *Tmem67*$^{-/-}$ E11.5 embryos of the MKS-like group of mutants, mostly likely due to either the lack of cilia or lack of functioning cilia that culminated in reduced Shh signalling.

In contrast, dorsoventral patterning of the caudal neural tube of E11.5 *Tmem67*$^{-/-}$ embryos with the JBTS-like phenotype did not have a visible roof plate defect and had robust expression of the floor plate marker Foxa2 (Fig. 4B). There was slight dorsal expansion for the ventral markers NKx2.1 and NKx6.1, and the dorsal marker Pax6 (Fig. 4B), indicating a mild ventralization of the neural tube in this group of mutant embryos which suggested that the bulbous 'JBTS-like' *Tmem67*$^{-/-}$ cilia (Fig. 3E) failed to constrain Shh signalling.

The MKS-like phenotype is associated with high de-regulated Wnt/β-catenin signalling

To investigate *in vivo* canonical Wnt (β-catenin-associated) signalling in 'MKS-like' *Tmem67*$^{-/-}$ mutants, we stained a meningocele-like anomaly (Fig. 5A) or abnormal nodular masses in the lateral ventricle (Supplementary Material, Fig. S3A) for IF microscopy. This revealed extensive increases in the overall levels of β-catenin (Fig. 5A, Supplementary Material, Fig. S3A) and near total loss of cilia at the developing neuroepithelial cell layer of the developing fourth ventricle (Fig. 5A). Although some primary cilia were still seen in the surrounding normal head mesoderm, cilia were lost from the cells forming the meningocele like defect (Fig. 5A).

Mouse embryonic fibroblasts (MEFs) derived from MKS-like mutant animals lacked primary cilia, or developed very short (<1 μm) cilia in 5% of cells, whereas 70% of *Tmem67*$^{+/+}$ MEFs had a single, uniform cilium of ∼2 μm in length (Fig. 5B). *Tmem67*$^{-/-}$ MEFs also developed a range of centrosomal defects comprising widely separated mother/daughter centrosomes and multiple centrosomes (Fig. 5B), consistent with previously reported defects following TMEM67/meckelin loss (31).

Western blot analysis of whole cell extracts (WCE) from MEFs confirmed higher basal levels of active, non-phosphorylated β-catenin, cyclin D1 (a downstream target of the Wnt/β catenin pathway) and phosphorylated Dishevelled-1 (Dvl-1, a key signalling modulator of Wnt pathways) (32–34) in *Tmem67*$^{-/-}$ compared with either *Tmem67*$^{+/-}$ or *Tmem67*$^{+/+}$ cells (Fig. 5C, Supplementary Material, Fig. S3B). Levels of phosphorylated Lrp6, a key co-receptor of the canonical Wnt/β catenin pathway, were markedly increased in *Tmem67*$^{-/-}$ compared with *Tmem67*$^{+/+}$ MEFs

Table 2. Summary of neurodevelopmental anomalies detected in *Tmem67*$^{-/-}$ mutants at the E13.5 to P0 stages of development

Phenotype(s)	*Tmem67*$^{-/-}$ mutant animals																			Total/19
	F6–F10											F>10								
	1	2	3	4	5	6	7	8	9	10	11	12	13	14	15	16	17	18	19	
Forebrain																				
Frontal meningocele/encephalocele			✓			✓		✓	✓	✓										5
Occipital defect			✓		✓	✓														3
Small forebrain	✓	✓		✓			✓	✓	✓	✓	✓	✓		✓	✓	✓	✓	✓	✓	15
Enlarged forebrain			✓		✓	✓							✓							4
Posterior fossa defects		✓		✓			✓													3
Cerebellar hypoplasia	✓	✓	✓	✓	✓	✓						✓	✓	✓	✓	✓	✓	✓	✓	16
Heterotopias					✓	✓	✓	✓	✓				✓							6
Deep interpeduncular fossa	✓		✓	✓		✓	✓													5
Phenotype group	J	J	M	D[a]	M	M	M	M	M	M	J	J	J	J	J	J	J	J	J	

In total, 31 *Tmem67*$^{-/-}$ animals were available for study, out of 133 animals of all genotypes. One *Tmem67*$^{-/-}$ mutant was resorbed, and the remaining 19 were examined morphologically or histologically. Individual animals (numbered 1–19) are separated on the basis of filial generation (F6–F10, or F>10, as indicated) after back-crossing onto the C57BL/6J genetic background. The phenotype group for each animal is indicated in the bottom row. Abbreviation: D, Dandy-Walker malformation; J, JBTS-like phenotype group; M, MKS-like phenotype group.
[a]Embryo sections shown in Supplementary Material, Fig. S2A.

following treatment with conditioned medium containing Wnt3a, a Wnt ligand known to activate canonical Wnt signalling (Fig. 5D). IF staining of β-catenin in MEFs detected higher levels of nuclear localization of active β-catenin in *Tmem67*$^{-/-}$ compared with *Tmem67*$^{+/+}$ MEFs following treatment with Wnt3a (Supplementary Material, Fig. S3C). Jouberin, a positive regulator of the canonical pathway that binds to β-catenin (35), also translocated to nuclei in this group of *Tmem67*$^{-/-}$ mutant cells (Supplementary Material, Fig. S3D). Finally, levels of active RhoA (a downstream mediator of the non-canonical Wnt signalling pathway) were reduced in *Tmem67*$^{-/-}$ compared with *Tmem67*$^{+/+}$ MEFs but could be increased by treatment with the non-canonical ligand Wnt5a (Fig. 5E).

We also used the TOPFlash assay to quantify the ability of *Tmem67*$^{+/+}$ and *Tmem67*$^{-/-}$ MEFs to respond to Wnt ligands. After transfection of the reporter constructs, treatment with Wnt3a stimulated basal levels of Wnt/β-catenin signalling by 5.3-fold in *Tmem67*$^{+/+}$ MEFs, but by 34.2-fold in mutant cells (Fig. 5F). As expected, Wnt5a on its own had no effect on this pathway (Fig. 5F). Transient co-transfection of a full-length wild-type human *TMEM67* construct rescued correct Wnt responses to Wnt3a stimulation (Fig. 5F).

The JBTS-like phenotype is associated with low de-regulated Wnt/β-catenin signalling, and increased non-canonical Wnt and Shh signalling

In contrast to MEFs from the 'MKS-like' group (Fig. 5B), MEFs derived from embryos of the JBTS-like group grew primary cilia, but over 40% of mutant cells had abnormally long (~10 μm) cilia (Fig. 6A) consistent with the structurally abnormal cilia seen by SEM (Fig. 3E). Staining of MEFs after Wnt3a treatment showed that nuclear translocation of β-catenin occurred normally as expected for *Tmem67*$^{+/+}$ cells, but in *Tmem67*$^{-/-}$ cells from the JBTS-like group nuclear accumulation of β-catenin failed to occur (Fig. 6B). To quantify the level of response in these cells to Wnt stimulation, we again used the TOPFlash assay and showed an aberrant low level of response in 'JBTS-like' *Tmem67*$^{-/-}$ MEFs following treatment with Wnt3a-conditioned medium (Fig. 6C). In contrast to 'MKS-like' MEFs (Fig. 5D), Wnt3a did not stimulate an increase in levels of β-catenin (Fig. 6D). Although Wnt3a stimulated increased levels of both non-phosphorylated and activated, phosphorylated Dvl-1 in 'MKS-like' MEFs (Supplementary Material, Fig. S3B), 'JBTS-like' *Tmem67*$^{-/-}$ MEFs down-regulated levels of Dvl-1 in response to this treatment (Fig. 6D). However, treatment of MEFs with Wnt5a induced the formation of prominent actin stress fibres in *Tmem67*$^{-/-}$ but not *Tmem67*$^{+/+}$ cells (Fig. 6E). Active RhoA levels were slightly increased in *Tmem67*$^{-/-}$ compared with *Tmem67*$^{+/+}$ cells, but were not affected by Wnt5a (Fig. 6E).

To further characterize the levels of Shh and Wnt/β-catenin signalling during neurodevelopment of 'JBTS-like' *Tmem67*$^{-/-}$ embryos, we used quantitative real-time PCR to measure the levels of *Shh* and *Axin2* transcripts in neocortical tissue dissected from E12.5, E15.5 and P0 animals. At E12.5, there was a statistically significant increase in *Shh* levels in *Tmem67*$^{-/-}$ neocortex compared with *Tmem67*$^{+/+}$ age-matched wild-type littermates (Fig. 6F), consistent with a loss of constraint for Shh signalling that could also cause the mild ventralization of the neural tube in 'JBTS-like' *Tmem67*$^{-/-}$ mutants (Fig. 4C). Conversely, canonical Wnt/β-catenin signalling (as measured by *Axin2*, a downstream target of the pathway) was significantly decreased in the P0 mutant cortex (Fig. 6F), consistent with the results in 'JBTS-like' MEFs (Fig. 6B–D).

The JBTS-like phenotype is associated with the loss of Dishevelled-1 localization at the basal body

Since the difference in de-regulated Wnt/β-catenin signalling levels appeared to distinguish between the 'MKS-like' and 'JBTS-like' groups of *Tmem67*$^{-/-}$ mutants, we next asked if this was reflected by the localization of Dvl-1, the downstream signalling modulator of Wnt pathways. In both 'MKS-like' *Tmem67*$^{-/-}$ and *Tmem67*$^{+/+}$ MEFs, Dvl-1 clearly

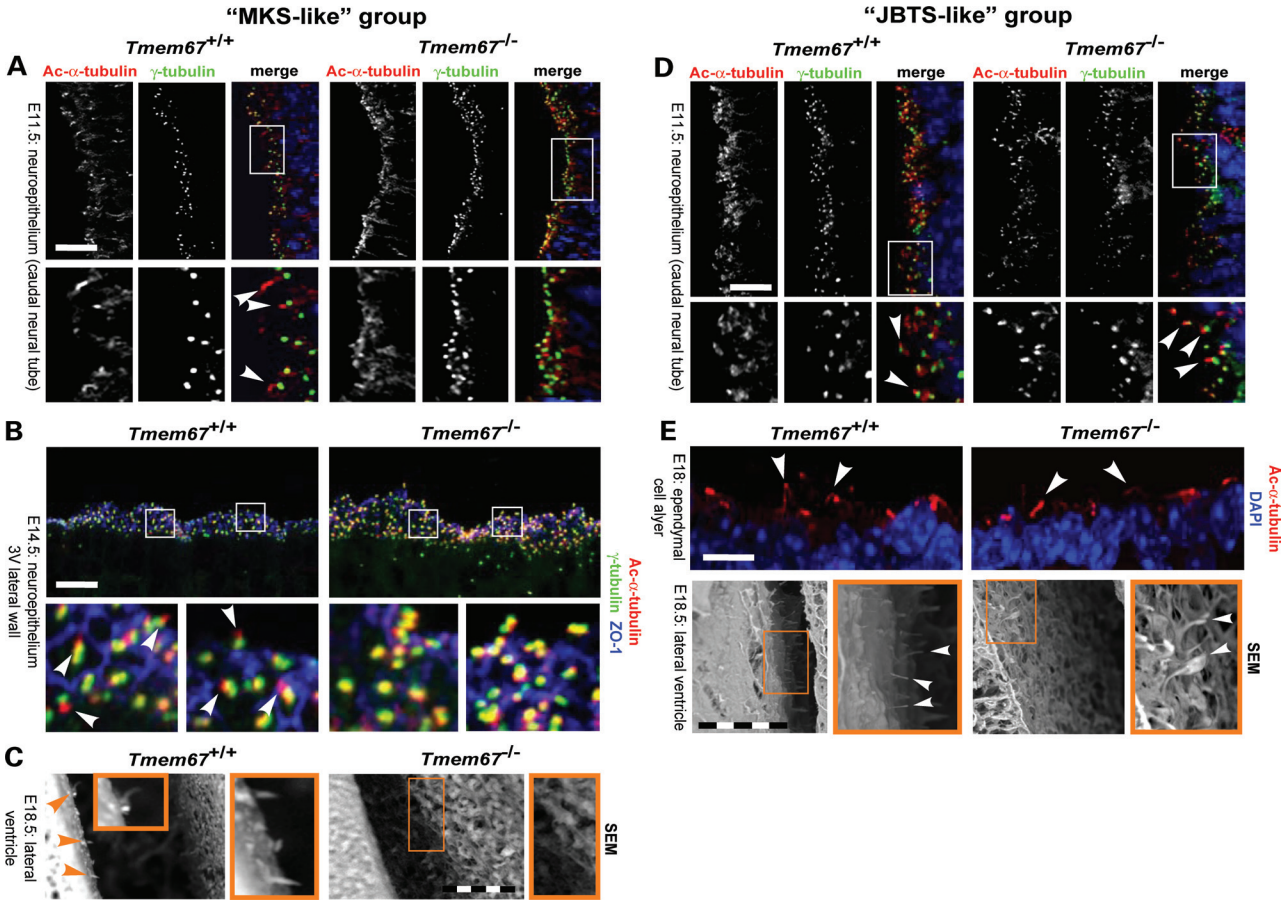

Figure 3. Different cilia defects in *Tmem67*$^{-/-}$ embryos with MKS-like and JBTS-like phenotypes: (**A,** top panels) Horizontal section of the developing E11.5 caudal neural tube in litter-mate *Tmem67*$^{+/+}$ and 'MKS-like' *Tmem67*$^{-/-}$ embryo at the level of the anterior limb buds stained for acetylated α-tubulin (red), centrosomes/basal bodies (γ-tubulin, green) and nuclei (DAPI, blue). (Bottom panels) Magnified insets (white frames) with primary cilia in the *Tmem67*$^{+/+}$ neural tube indicated by arrowheads. Scale bar = 10 μm. (**B**) E14.5 neuroepithelium of the lateral wall of the third ventricle (3V) in litter-mate *Tmem67*$^{+/+}$ and 'MKS-like' *Tmem67*$^{-/-}$ embryo stained as for (A). Scale bar = 10 μm. (**C**) SEM images of E18.5 lateral ventricles showing loss of primary cilia and disruption in the planar polarization of the ependymal cell layer in an 'MKS-like' *Tmem67*$^{-/-}$ embryo. Magnified insets (orange frames) show detail of cilia (arrowheads) in a littermate *Tmem67*$^{+/+}$ embryo. Scale bar = 50 μm with 10 μm subdivisions. (**D,** top panels) Horizontal sections as in (A) for littermate *Tmem67*$^{+/+}$ and 'JBTS-like' *Tmem67*$^{-/-}$ embryo stained for acetylated α-tubulin (red), centrosomes/basal bodies (γ-tubulin, green) and nuclei (DAPI, blue). (Bottom panels) Magnified insets (white frames) with primary cilia indicated by arrowheads. Scale bar = 10 μm. (**E**) IF microscopy (top panels) and SEM images (bottom panels) of E18.5 lateral ventricles showing the presence of abnormal, bulbous cilia and defective planar organization of the ependymal layer in 'JBTS-like' *Tmem67*$^{-/-}$ embryos. Magnified insets (orange frames) show detail of cilia (arrowheads). Scale bar = 50 μm with 10 μm subdivisions.

co-localized with basal bodies (Fig. 7A) as expected (36). However, in 'JBTS-like' *Tmem67*$^{-/-}$ cells, Dvl-1 co-localization with basal bodies was markedly reduced (Fig. 7B), consistent with the low de-regulated Wnt/β-catenin signalling observed in mutant embryos with this phenotype (Fig. 6B–D and F). *In vitro* co-immunoprecipitations demonstrated a biochemical interaction between Dvl-1 and meckelin/TMEM67 (Fig. 7C). However, a pathogenic in-frame deletion (p.919delF) in the cytoplasmic coiled-coil domain of meckelin/TMEM67 (37) reduced the interaction with Dvl-1, suggesting that either meckelin/TMEM67 or an associated ciliary transition zone protein is essential for the normal localization of Dvl-1.

DISCUSSION

Ciliopathies are a group of developmental disorders with overlapping clinical phenotypes, but for allelic ciliopathies such as MKS and JBTS the mechanism of the variability of phenotype expressivity remains unclear. Allelism at a primary causative locus is not thought to solely explain this variability, implicating the effect of additional modifier alleles (38). We now describe the study of the *Tmem67*$^{tm1(Dgen/H)}$ mouse model for both MKS and JBTS, with targeted mutagenesis of the *Tmem67* gene (also known as *Mks3*; Supplementary Material, Fig. S1A). *Tmem67*$^{-/-}$ mutants on an incipient congenic (F6–F10) C57BL/6J genetic background had typical ciliopathy features, comprising renal cystic dysplasia and hepatic developmental defects that are diagnostic for MKS in human patients. *Tmem67*$^{-/-}$ mutants also manifested a complex and variable suite of neurodevelopment phenotypes (Table 1 and 2), in contrast to the mild hydrocephaly reported for both the *Wpk* rat (39) and the *bpck* mouse models (40). In fully congenic (F > 10) embryos and pups that survived to P0 or P1, neurodevelopmental phenotypes were less variable and pathognomonic for JBTS (Table 2). The *Tmem67*$^{tm1(Dgen/H)}$

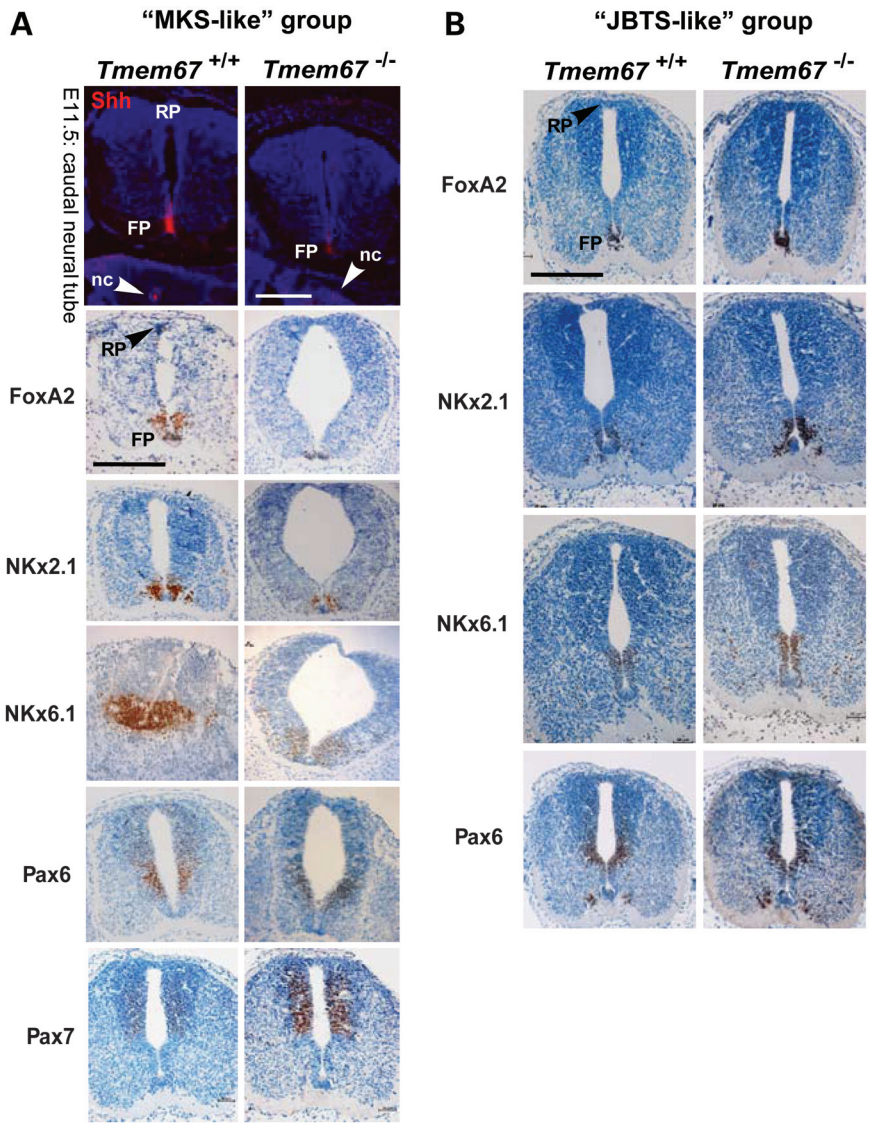

Figure 4. Defective dorsoventral patterning and Shh signalling in *Tmem67*$^{-/-}$ mutants: (**A**) loss of Shh signalling and dorsalization of the caudal neural tube in 'MKS-like' embryos. (Top panel) Shh protein expression (red) at the notochord (nc, arrowheads) and induced expression at the floor plate (FP) in the *Tmem67*$^{+/+}$ embryo. (Bottom panels) IHC staining for the indicated dorsoventral patterning markers and haemotoxylin counterstaining. Note the variable thinning of the roof plate (RP) in *Tmem67*$^{-/-}$ embryos. Scale bar = 100 μm. (**B**) Activation of the Shh signalling pathway and mild ventralization defects in 'JBTS-like' embryos using IHC staining for the indicated dorsoventral patterning markers. Note the absence of any roof plate defect in *Tmem67*$^{-/-}$ embryos.

mouse model has been described previously (22), and in the present study, *Tmem67*$^{-/-}$ mouse pups died at birth or during the early postnatal period, consistent with previous results (22). However, in contrast to our study, Garcia-Gonzalo *et al.* (22) described *Tmem67*$^{-/-}$ mutants with a normal external morphology and manifesting renal cystic dysplasia at E18.5, but did not perform extensive analyses of neurodevelopmental phenotypes and did not note the variability of the *Tmem67*$^{-/-}$ phenotype.

We separated the neurodevelopmental phenotypes in *Tmem67*$^{-/-}$ mutants on the basis of severity. The first group had an 'MKS-like' phenotype with the presence of cranial neural tube defects early in development (Fig. 1A–C), and the later development of a frontal encephalocele/meningocele (Fig. 1E) and prosencephalon dysgenesis (Fig. 1F), all of which are features of human MKS (3,41). The second 'JBTS-like' group had milder defects of the posterior fossa resembling clinical features of JBTS patients (Fig. 2B, Supplementary Material, Fig. S2A). Furthermore, there was inter-individual variation in these phenotypes, even for *Tmem67*$^{-/-}$ mutant littermates (Supplementary Material, Fig. S2B). The *Tmem67* mouse is therefore a unique model for severe human ciliopathies and their phenotypic variability, since the *Tmem67*$^{-/-}$ mutants fully recapitulate the human MKS type 3 clinical presentation (42) and vermian hypoplasia (Fig. 2D), an essential diagnostic finding in JBTS patients (43).

In the present study, we now show that TMEM67/meckelin has complex roles in regulating canonical Wnt/β-catenin and Shh signalling in the developing brain. TMEM67/meckelin

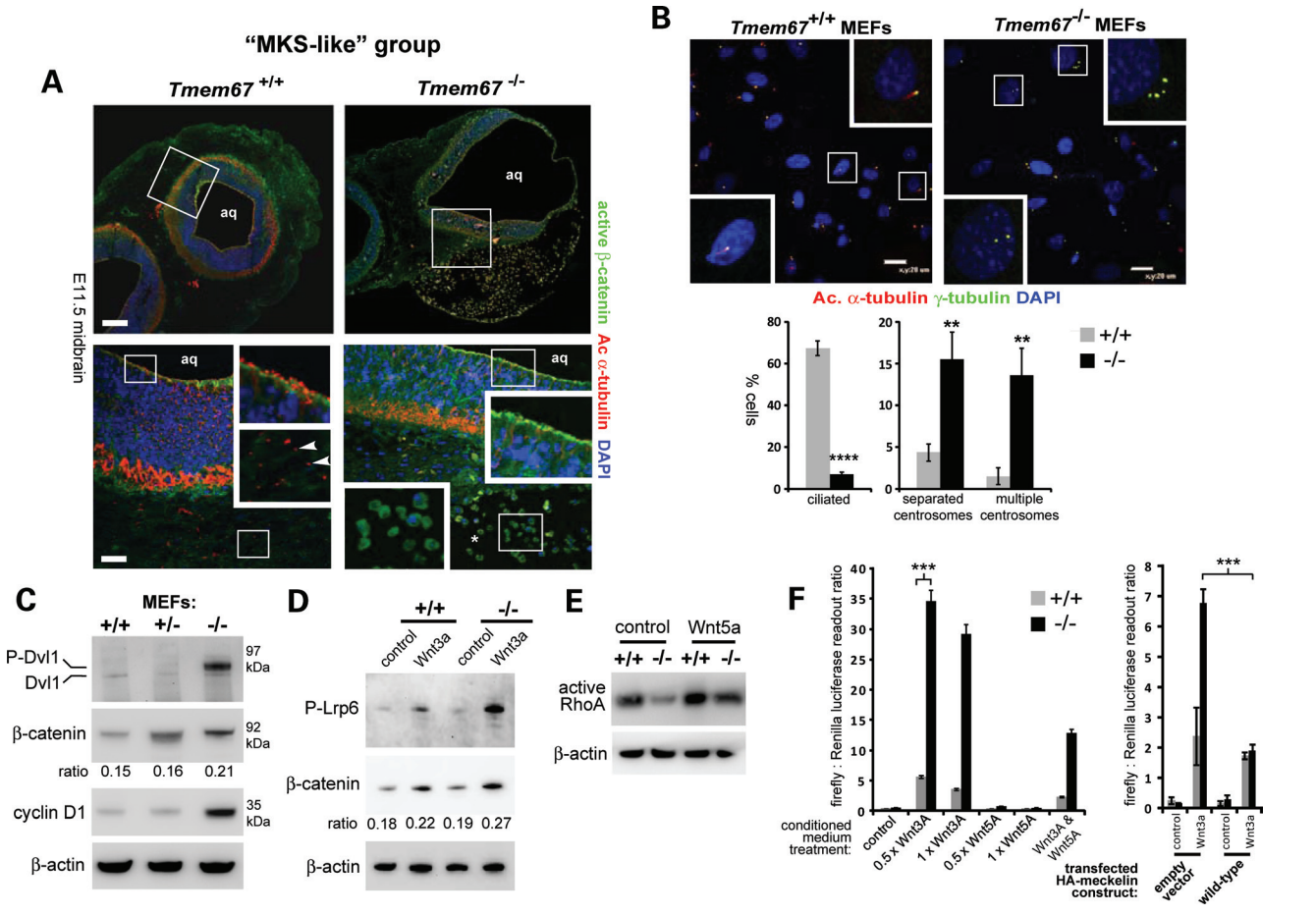

Figure 5. *In vivo* and *in vitro* up-regulated canonical Wnt/β-catenin signalling defects in *Tmem67*$^{-/-}$ embryos with MKS-like phenotypes: (**A,** top panels) IF confocal microscopy of horizontal midbrain sections of E11.5 embryos, with regions magnified in the bottom panels indicated by white frames in top panels. The *Tmem67*$^{-/-}$ mutant shows a prominent meningocele (bottom panel, asterisk), stained for the primary ciliary axoneme (acetylated α-tubulin, red), activated β-catenin (green) and nuclei (DAPI, blue). Magnified insets (white frames) show detail of primary cilia (arrowheads) in the *Tmem67*$^{+/+}$ embryo; 4V, fourth ventricle. Scale bar = 20 μm. (**B**) IF microscopy of *Tmem67*$^{+/+}$ MEFs and *Tmem67*$^{-/-}$ MEFs derived from embryos with an MKS-like phenotype, stained for acetylated α-tubulin (red), centrosomes/basal bodies (γ-tubulin, green) and nuclei (DAPI, blue). Magnified insets (white frames) show detail of ciliogenesis and centrosomal defects in *Tmem67*$^{-/-}$ MEFs. Three separate MEF lines for both genotypes were derived and consistently assayed at passage 3. Bar graphs quantify ciliogenesis (presence of a cilium defined as a single, uniform axoneme >2 μm in length; absence defined as <1 μm or complete failure of ciliogenesis) and centrosomal/basal body defects (>5 μm separation, or multiple centrosomes/dispersal of pericentriolar material). Scale bars = 20 μm. (**C**) Immunoblotting of whole cell lysates extracted from wild-type *Tmem67*$^{+/+}$ (+/+), heterozygous *Tmem67*$^{+/-}$ (+/−) and mutant 'MKS-like' *Tmem67*$^{-/-}$ (−/−) MEFs for Dishevelled-1 (Dvl1, phosphorylated P-Dvl1 also indicated), total β-catenin and cyclin D1. Immunoblotting for β-actin is the loading control. The ratio of β-catenin band intensity: loading control band intensity is indicated. (**D**) Whole cell lysates from MEFs of the indicated genotypes stimulated with Wnt3a-conditioned media immunoblotted for phosphorylated (P)-Lrp6 and total β-catenin. The ratio of β-catenin band intensity: loading control band intensity ('ratio') is indicated below the β-catenin panel. (**E**) Whole cell lysates from MEFs of the indicated genotypes treated with Wnt5a and assayed for active RhoA levels by a pulldown assay. (**F**) Bar graph on left: TOPFlash assays for *Tmem67*$^{+/+}$ (grey) and 'MKS-like' *Tmem67*$^{-/-}$ (black) MEFs following treatment with the indicated conditioned media. Bar graph on right: dysregulated canonical Wnt signalling in 'MKS-like' *Tmem67*$^{-/-}$ cells following Wnt3a treatment is rescued by cotransfection with wild-type HA-TMEM67 expression construct but not empty vector control. Values shown are means of at least four independent replicates.

is required for correct ciliogenesis in the CNS, and in MEFs derived from 'MKS-like' (Fig. 1) and 'JBTS-like' (Fig. 2) groups of animals: the MKS-like group failed to form cilia (Figs 3A–C, 5A and B), whereas a proportion of cilia in the JBTS-like group did form (Fig. 3D) but were structurally abnormal (Figs 3E and 6A). These ciliary phenotypes directly correlated with the type of de-regulation that we observed for both canonical Wnt/β-catenin and Shh signalling in these two groups. In the 'MKS-like' group, TMEM67/meckelin loss caused a very high de-regulated level of Wnt/β-catenin signalling both *in vivo* (Figs 1G and 5A; Supplementary Material, Fig. S3A) and *in vitro* (Fig. 5C, D, F). This is entirely consistent with previous reports that cilia act as a negative regulator of the canonical Wnt/β-catenin signalling (18,19,44). In contrast, cells that grew abnormally long cilia failed to activate the canonical pathway (Fig. 6B–D) and β-catenin translocation to the nucleus was disturbed (Fig. 6B), indicating that active β-catenin translocation into the nucleus is a process that requires a functioning cilium in the JBTS-like disease state. This finding is also consistent with a previous report describing a mouse model of JBTS, since the *Ahi1* mouse model developed reduced canonical

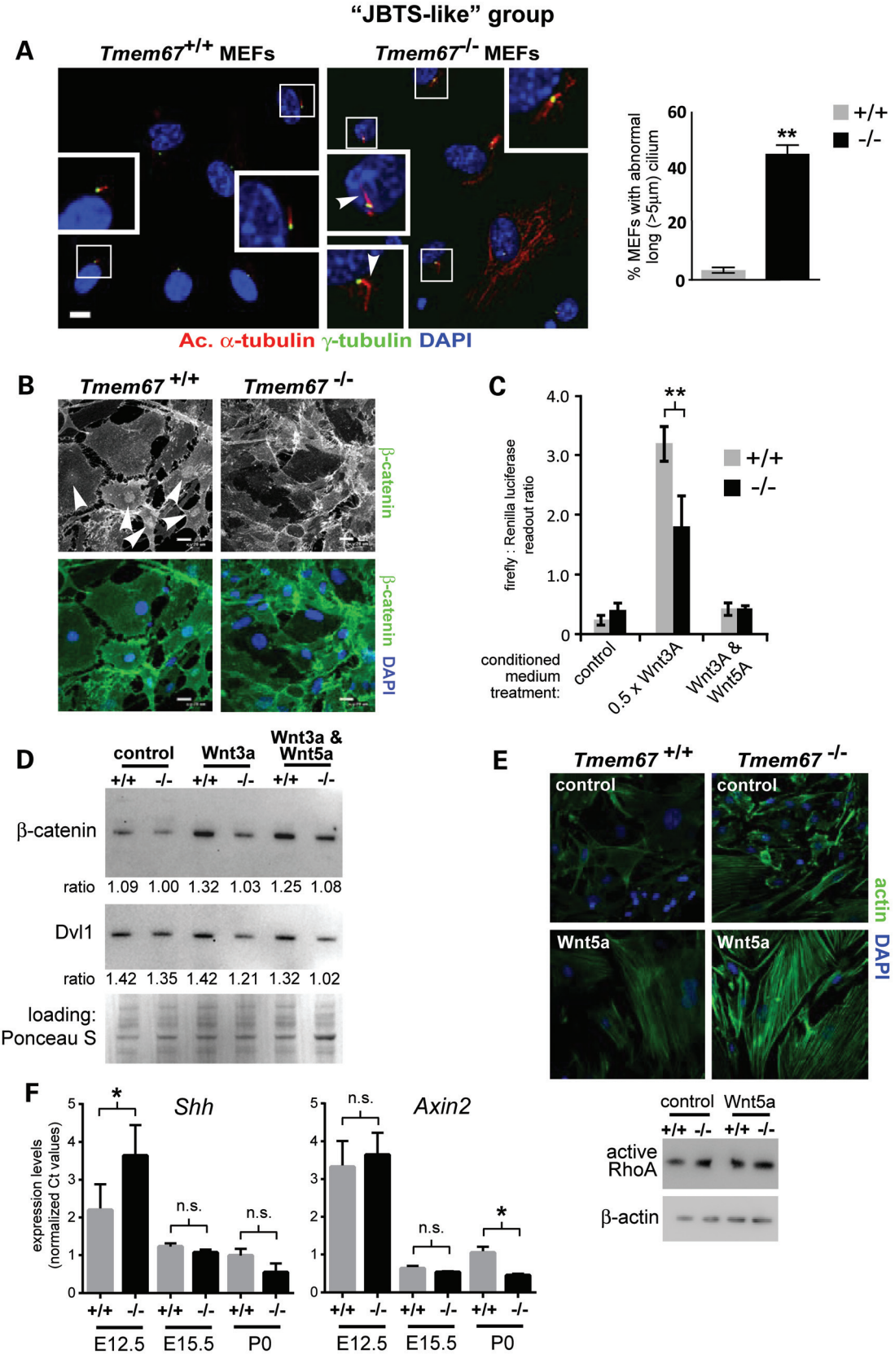
"JBTS-like" group
A
Tmem67+/+ MEFs
Tmem67-/- MEFs
Ac. α-tubulin γ-tubulin DAPI
% MEFs with abnormal long (>5μm) cilium
+/+
-/-
**
B
Tmem67 +/+
Tmem67 -/-
β-catenin
β-catenin DAPI
C
firefly : Renilla luciferase readout ratio
conditioned medium treatment:
control
0.5 x Wnt3A
Wnt3A & Wnt5A
D
control
Wnt3a
Wnt3a & Wnt5a
β-catenin
ratio 1.09 1.00 1.32 1.03 1.25 1.08
Dvl1
ratio 1.42 1.35 1.42 1.21 1.32 1.02
loading: Ponceau S
E
Tmem67 +/+
Tmem67 -/-
control
Wnt5a
actin DAPI
control Wnt5a
active RhoA
β-actin
F
Shh
Axin2
expression levels (normalized Ct values)
n.s.
E12.5
E15.5
P0

Wnt signalling accompanied with reduced proliferation in the developing cerebellum, although cilia morphology was not affected in this model (45). The aberrant down-regulation of canonical Wnt/β-catenin signalling in *Tmem67*$^{-/-}$ during later development (Fig. 6F), therefore, provides an explanation of the vermian hypoplasia in the 'JBTS-like' group.

Neuroepithelial cells of the ventricular zone in the developing 'MKS-like' *Tmem67*$^{-/-}$ E11.5 neural tube did not form cilia (Fig. 3A), and, as expected, we saw a reduction in the number of ventral neuronal and floor plate cell types in the cervical neural tube (Fig. 4A). The loss of cilia in the 'MKS-like' group therefore suppressed the Shh pathway (30), leading to typical ciliopathy mouse mutant phenotypes of neural tube dorsalization (Fig. 4A and B). This is consistent with a similar loss of Shh-dependent ventral neural cell types in mutants that lack IFT complex B proteins (for example *Ift88* or *Ift172*) or *Shh* genes (46–48). In contrast, 'JBTS-like' *Tmem67*$^{-/-}$ embryos at E11.5 had a mild ventralization defect of the caudal neural tube (Fig. 4C) and a significant increase in *Shh* expression in the E12.5 neocortex (Fig. 6f). These indicated a failure in constraint of the Shh signalling pathway despite the presence of (albeit structurally abnormal) primary cilia (Figs 3E and 6A).

Other mutant models with ventralized neural tube patterning, such as *Rab23* and *Tulp3* mutants, implicate defective Gli transcription factor processing since Rab23 and Tulp3 normally function to either inhibit the activation of Gli2, or repress Shh in the absence of ligand in a Gli2-dependent but Smo-independent manner (49–51). Future work should therefore test if TMEM67/meckelin can also act as a negative modulator of the Shh pathway and stabilize activated full-length Gli3 proteins, at least in animals of the 'JBTS-like' group, by mediating correct ciliary trafficking at the transition zone that is required for proteolytic processing of Gli transcription factors (52). TMEM67/meckelin is enriched at the base of the primary cilium in the ciliary transition zone (22,26), which suggests a working model where trafficking of Gli proteins between compartments in the cilium regulates their accessibility to TMEM67/meckelin (and other transition zone proteins that modulate signalling pathways). This process would then determine the fate of Gli proteins and the activity of the Shh pathway. In support of this interpretation, we observed an analogous process for modulation of canonical Wnt/β-catenin signalling. Dvl-1 co-localization with the basal body was maintained in the 'MKS-like' disease state (Fig. 7A), associated with Dvl-1 phosphorylation and activation (Fig. 5C). However, in the 'JBTS-like' disease state, Dvl-1 co-localization with the basal body was reduced (Fig. 7B), which would be expected to disrupt normal ciliary trafficking and prevent the activation of the Wnt/β-catenin signalling pathway. Interestingly, the pathogenic in-frame deletion mutation p.919delF in TMEM67/meckelin (37) reduced the interaction with Dvl-1 (Fig. 7C) and abrogated canonical Wnt/β-catenin responses following treatment with Wnt3a (37).

The modifier allele hypothesis provides an attractive explanation for the variability of phenotype expressivity in *Tmem67*$^{-/-}$ embryos, and the differing Shh and Wnt signalling responses in the 'MKS-like' and 'JBTS-like' phenotypic groups. In support of this observation, recent studies have described both general and specific buffering or compensatory systems that combine to determine the outcome of an inherited mutation leading to inter-individual variation (53). The origin of inter-individual variation in levels of gene expression includes ancestral gene duplications and marked variation in the induction of the molecular chaperones such as Hsp90 that appear to act as random buffers of genetic variation (54). However, such mechanisms do not preclude the effect of environmental factors on inter-individual levels of gene expression. We also noted that more severely affected *Tmem67*$^{-/-}$ embryos were invariably at distal locations in the left and right uterine horns of pregnant dams, suggesting an effect due to variations in placental blood supply (data not shown). The molecular causes of the switch between aberrant up- and down-regulation of signalling in the *Tmem67* knock-out line remain unknown, but are likely to include the effect of modifier alleles and stochastic effects that are likely to be context-dependant or highly sensitive to any environmental cues. We speculate that modifier alleles in the TMEM67/meckelin-Dvl-1 signalling axis, or other signalling modulators at the transition zone, may contribute to this phenotypic variation. The congenic *Tmem67* line therefore provides a unique model system to elucidate the pathogenesis of MKS and JBTS phenotypic variability.

MATERIALS AND METHODS

Animals

The animal studies described in this paper were carried out under the guidance issued by the Medical Research Council in *Responsibility in the Use of Animals for Medical Research* (July 1993) in accordance with UK Home Office regulations under the Project Licence No. PPL40/3349. C57BL/6J;129P2-*Tmem67*$^{tm1(Dgen/H)}$ heterozygous knock-out mice were derived from a line generated by Deltagen Inc. and made available from MRC Harwell through the European

Figure 6. Down-regulated canonical Wnt/β-catenin signalling in *Tmem67*$^{-/-}$ embryos with JBTS-like phenotypes: (**A,** left panel) IF confocal microscopy of *Tmem67*$^{+/+}$ MEFs and *Tmem67*$^{-/-}$ MEFs derived from embryos with a JBTS-like phenotype, stained for acetylated α-tubulin (red), γ-tubulin (green) and nuclei (blue). Magnified insets (white frames) show detail of cilia. (Right panel) The bar graph quantifies the number of abnormally long cilia (>5 μm). Scale bar = 20 μm. (**B**) MEFs stimulated with Wnt3a and stained for β-catenin (green) and nuclei (blue) show normal nuclear translocation of β-catenin in *Tmem67*$^{+/+}$ MEFs (arrowheads) but not in *Tmem67*$^{-/-}$ MEFs. (**C**) TOPFlash assays in *Tmem67*$^{+/+}$ and 'JBTS' *Tmem67*$^{-/-}$ MEFs following treatment with the indicated conditioned media. Values shown are means of at least four independent replicates. (**D**) Whole cell lysates extracted from wild-type *Tmem67*$^{+/+}$ (+/+) and mutant 'JBTS-like' *Tmem67*$^{-/-}$ (−/−) MEFs, following treatment with the indicated conditioned media, were immunoblotted for β-catenin and Dishevelled-1 (Dvl-1), with Ponceau S staining as the loading control. The ratios of either β-catenin or Dvl-1 band intensities: loading control band intensity ('ratio') are indicated beneath the appropriate panel. (**E,** top panel) IF confocal microscopy of *Tmem67*$^{+/+}$ and 'JBTS' *Tmem67*$^{-/-}$ MEFs for phalloidin to visualize F-actin following treatment with either control- or Wnt5a-conditioned media as indicated. (Bottom panel) Whole cell lysates from MEFs of the indicated genotypes treated with Wnt5a and assayed for active RhoA levels. (**F**) qRT-PCR results for *Tmem67*$^{+/+}$ (grey) and JBTS-like *Tmem67*$^{-/-}$ (black) cortical tissue at embryonic ages E12.5, E15.5 and P0 as indicated, showing the expression levels of *Shh* (left panel) and *Axin2* (right panel). Values shown are means of three independent biological replicates.

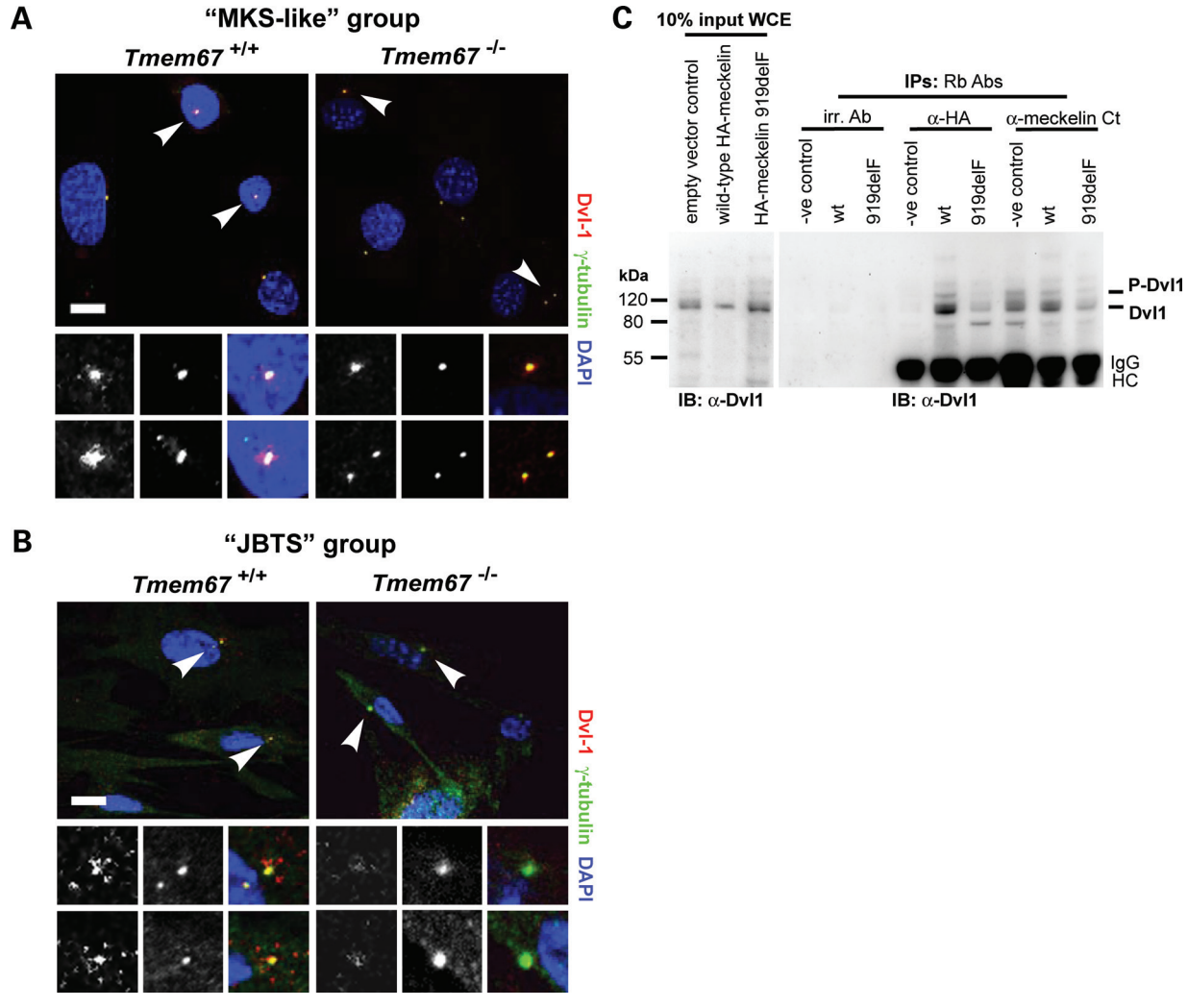

Figure 7. Disruption of the TMEM67/meckelin-Dishevelled-1 axis is associated with the JBTS-like phenotype. (**A**) IF confocal microscopy of *Tmem67*$^{+/+}$ MEFs and *Tmem67*$^{-/-}$ MEFs derived from embryos with an MKS-like phenotype, stained for Dvl-1 (red), γ-tubulin (green) and and nuclei (blue). Arrowheads indicate the cells magnified in the insets below. Scale bar = 10 μm. (**B**) *Tmem67*$^{+/+}$ MEFs and *Tmem67*$^{-/-}$ MEFs derived from embryos with a JBTS-like phenotype, stained as in (A). Scale bar = 10 μm. (**C**) Immunoprecipitation (IP) of endogenous Dvl-1 by wild-type TMEM67/meckelin. HEK293 cells were transfected with empty vector negative control (control), wild-type HA-meckelin (wt) or p.F919del mutant HA-meckelin (919delF) constructs. Expression of HA-tagged proteins has been determined previously by immunoblotting with anti-HA (Fig. 2C, ref. 26). (Left panel) 10% of total input WCE for each IP is indicated. (Right panel) Affinity-purified 'Ct Ab' anti-meckelin antibody against the C-terminus, and anti-HA rabbit polyclonal (Rb Abs) against epitope-tagged wild-type HA-meckelin, preferentially pull-down endogenous Dvl-1. Expression of the p.F919del mutant HA-meckelin (919delF) abrogated or prevented interaction with Dvl-1. IP for an irrelevant monoclonal antibody (irr. Ab.) did not pull-down Dvl-1.

Mutant Mouse Archive, http://www.emmanet.org/ (strain number EM:02370). The targeted *β-Gal-neo* ('*geo*') construct inserts downstream of exon one of the *Tmem67* gene (Supplementary Material, Fig. S1A). Genotyping was done by PCR on DNA extracted from tail tips or the yolk sac of the E11.5 embryos, or tail or ear biopsies of older embryos and adult mice, respectively. Animals were back-crossed onto the C57BL/6J genetic background for five filial generations (F5) before performing the anatomical and functional characterization.

Preparation of tissue sections, histology and immunohistochemistry

Mouse embryos or dissected tissues were fixed in 4% (w/v) para-formaldehyde and embedded in paraffin wax. Thin sections (4 μm) were cut onto 'Superfrost Plus' slides (VWR International Ltd.) and were deparaffinized and rehydrated by standard methods. Sections were stained with haematoxylin and eosin (BDH Chemicals Ltd.) for 2 min, then dehydrated in ethanol, cleared in xylene and mounted in DPX. For immunohistochemistry, tissue sections were deparaffinized and rehydrated through passing in xylene and desending grades of ethanol. Epitope recovery was obtained by boiling in 1 mM EDTA pH 8.0 for 2 min using pressure cooker, followed by 30 min cooling. Blocking and application of primary antibodies was as described (55). Appropriate HRP-conjugated secondary antibodies (Dako Inc.) were used (final dilutions of ×10 000–25 000). Sections were developed in 'Sigma Fast' 3,3′-diaminobenzidine (DAB) with $CoCl_2$ enhancer and counterstained with Mayer's haematoxylin (Sigma-Aldrich Co. Ltd.).

Cells

Human embryonic kidney (HEK293) cells were grown in Dulbecco's minimum essential medium (DMEM)/Ham's F12 supplemented with 10% fetal calf serum at 37°C/5% CO_2. The derivation and culture of MEFs have been described previously (56). The MEFs were derived from E15.5 embryos in both phenotype groups, using identically similar experimental procedures, and assayed consistently at identical passage numbers of 2 or 3. Three separate MEF lines for both phenotype groups were derived and used in assays. MEFs were grown in DMEM/Ham's F12 supplemented with 10% fetal calf serum and 1% penicillin streptomycin at 37°C/5% CO_2.

Cloning, plasmid constructs and transfections

Full-length human *MKS3* was cloned into the pCMV-HA vector as described previously (37) and verified by bidirectional DNA sequencing. For transfection with plasmids, cells at 80% confluency were transfected using Lipofectamine 2000 (Invitrogen Inc.) according to the manufacturer's instructions and as described previously (57).

Antibodies

The following primary antibodies were used: mouse anti-acetylated-α-tubulin clone 6-11B-1 (Sigma-Aldrich Co. Ltd.); rabbit-anti-γ-tubulin and mouse anti-β actin clone AC-15 (Abcam Ltd.); mouse anti-Dvl-1 clone 3F12 and mouse anti-cyclin D1 clone A-12 (Santa Cruz Biotechnology Inc.); mouse anti-activated β-catenin (anti-ABC, clone 8E7) and mouse anti-Ki67 (Merck Millipore Inc.); and mouse anti-neuron-specific β3-tubulin (Tuj1) clone TU-20, rabbit anti-phospho-LRP6 (Ser1490), rabbit anti-β-catenin (Cell Signaling Technology Inc.). The monoclonal antibodies anti-Shh clone 5E1, anti Fox2A clone 4C7, anti-Pax6, anti-Pax7, anti-NKx6.1 clone F55A10 and anti-NKx2.2 clone 74.5A5 were obtained from the Developmental Studies Hybridoma Bank developed under the auspices of the NICHD and maintained by the University of Iowa, Department of Biology, Iowa City, USA. Rabbit anti-TMEM67/meckelin N-terminus or C-terminus (TMEM67 Nt or Ct, 'Nt Ab' or 'Ct Ab' in Supplementary Material, Fig. S1A) have been described previously (57). Secondary antibodies were Alexa-Fluor 350-, Alexa-Fluor 488-, Alexa-Fluor 568- and Alexa-Fluor 594-conjugated goat anti-mouse IgG and goat anti-rabbit IgG (Molecular Probes Inc.). Alexa-Fluor 488 phalloidin conjugate (Life Technologies Corp.) was used to visualize F-actin.

Immunofluorescence and confocal microscopy

Cells were seeded at 1.5×10^5 cells/well on glass cover slips in six-well plates and fixed in ice-cold methanol (5 min at −20°C) or 2% paraformaldehyde (20 min at room temperature). Permeabilization, blocking methods and immunofluorescence staining were essentially as described previously (9). Primary antibodies were used at final dilutions of ×200–1000. Secondary antibodies were diluted ×500. Confocal images were obtained using a Nikon Eclipse TE2000-E system, controlled and processed by EZ-C1 3.50 (Nikon Inc.) software. Images were assembled using Adobe Illustrator CS2.

WCE preparation and immunoblotting

WCE from confluent MEFs were prepared by standard methods. 10 μg WCE total soluble protein was analysed by SDS–PAGE (using 4–12% acrylamide gradient gels) and western blotting according to standard protocols using either rabbit polyclonal antisera (final dilutions of ×200–1000) or mAbs (×1000–5000). Appropriate HRP-conjugated secondary antibodies (Dako Inc.) were used (final dilutions of ×10 000–25 000) for detection by the enhanced chemiluminescence 'Femto West' western blotting detection system (Pierce Inc.). Levels of β-actin were used as a loading control for all immunoblotting experiments.

Canonical Wnt activity (TOPFlash) luciferase assays

MEFs were co-transfected with 0.5 μg TOPFlash firefly luciferase construct (or FOPFlash, as a negative control); 0.5 μg of expression constructs (pCMV HA-TMEM67, or empty pCMV-HA control); and 0.05 μg of pRL-TK internal control *Renilla* luciferase reporter construct (Promega Corp). Cells were treated with Wnt3a- or Wnt5a-conditioned media (58). Luciferase activities were assayed with the Dual-Luciferase Reporter Assay system (Promega Corp.) on a Mithras LB940 (Berthold Technologies Inc.) luminometer. Raw readings were normalized with *Renilla* luciferase values, and the results reported are from at least four independent biological replicates.

RhoA activation assays

The activated GTP-bound isoform of RhoA was specifically assayed in pull-down assays using a GST fusion protein of the Rho effector rhotekin (Cytoskeleton, Inc.), using conditions recommended by the manufacturers, and as described previously (37).

Gene expression analyses by quantitative real-time PCR

For the relative quantification of gene expression, we used the standard curve method of quantitative real-time PCR. Total RNA (1 μg) was reverse transcribed using the Superscript III First-Strand cDNA System (Invitrogen Inc.). PCR analysis of cDNA was performed using dHPLC-purified primers (Sigma-Aldrich Ltd.) specific for mouse *Shh* and *Axin2*. Primer sequences are available upon request. Each reaction was run in triplicate. Amplimer levels were quantified continuously with the SYBR GreenER qPCR system (Invitrogen Inc.) using an ABI 7500 instrument, as described previously (8). Beta-actin was amplified for normalization.

Statistical analyses

Normal distribution of data (TOPFlash activities, cilia length measurements) was confirmed using the Kolmogorov–Smirnov test (GraphPad Prism). Pairwise comparisons were analysed with Student's two-tailed *t*-test using InStat

(GraphPad Prism). Results reported are from at least three independent biological replicates. Error bars on bar graphs indicate SEM. The statistical significance of pairwise comparisons shown on bar graphs is indicated by: n.s., not significant, $^{*}P < 0.05$, $^{**}P < 0.01$, $^{***}P < 0.001$ and $^{****}P < 0.0001$. For cell populations, a minimum of 150 cells were counted from 10 separate fields of view. Contingency tables were analysed with Pearson's chi-squared test, using two degrees of freedom (GraphPad Prism).

SUPPLEMENTARY MATERIAL

Supplementary Material is available at *HMG* online.

ACKNOWLEDGEMENTS

We thank A. Monk, K. Passam and T. Simpson of Nikon UK Ltd. for technical support and advice on confocal microscopy. We are very grateful to D. Evans, J. Bilton, C. McCartney and M. Reay for technical support. We thank R. T. Moon, University of Washington, for the TOPFlash and FOPFlash constructs. The anti-Gli3 antibodies were the kind gift of S. Scales, Genentech, CA, USA. The anti-jouberin antibody was the kind gift of J. Gleeson, University of California Santa Cruz, CA, USA.

Conflict of Interest statement. None declared.

FUNDING

This work was supported by the UK Medical Research Council (project grant G0700073 to C.A.J.), Kid's Kidney Research (to C.A.J.) and an Egyptian Government Scholarship (to Z.A.A.). The research also received funding from the European Community's Seventh Framework Programme FP7/2009 under grant agreement no: 241955 SYSCILIA. Access to the *Tmem67*$^{tm1Dgen/H}$ line was funded by the Wellcome Trust Knock-out Mouse Resource scheme (grant ME041596 to C.A.J. and C.F.I.). The funders had no role in study design, data collection and analysis, decision to publish or preparation of the manuscript.

REFERENCES

1. Alexiev, B.A., Lin, X., Sun, C.-C. and Brenner, D.S. (2006) Meckel-Gruber syndrome: pathologic manifestations, minimal diagnostic criteria, and differential diagnosis. *Arch. Pathol. Lab. Med.*, **130**, 1236–1238.
2. Salonen, R. and Paavola, P. (1998) Meckel syndrome. *J. Med. Genet.*, **35**, 497–501.
3. Ahdabbarmada, M. and Claassen, D. (1990) A distinctive triad of malformations of the central-nervous-system in the Meckel-Gruber syyndrome. *J. Neuropathol. Exp. Neurol.*, **49**, 610–620.
4. Paetau, A., Salonen, R. and Haltia, M. (1985) Brain pathology in the Meckel syndrome—a study of 59 cases. *Clin. Neuropathol.*, **4**, 56–62.
5. Baala, L., Romano, S., Khaddour, R., Saunier, S., Smith, U.M., Audollent, S., Ozilou, C., Faivre, L., Laurent, N., Foliguet, B. *et al.* (2007) The Meckel-Gruber syndrome gene, MKS3, is mutated in Joubert syndrome. *Am. J. Hum. Genet.*, **80**, 186–194.
6. Patel, S. and Barkovich, A.J. (2002) Analysis and classification of cerebellar malformations. *Am. J. Neuroradiol.*, **23**, 1074–1087.
7. Kyttala, M., Tallila, J., Salonen, R., Kopra, O., Kohlschmidt, N., Paavola-Sakki, P., Peltonen, L. and Kestila, M. (2006) MKS1, encoding a component of the flagellar apparatus basal body proteome, is mutated in Meckel syndrome. *Nat. Genet.*, **38**, 155–157.
8. Smith, U.M., Consugar, M., Tee, L.J., McKee, B.M., Maina, E.N., Whelan, S., Morgan, N.V., Goranson, E., Gissen, P., Lilliquist, S. *et al.* (2006) The transmembrane protein meckelin (MKS3) is mutated in Meckel-Gruber syndrome and the wpk rat. *Nat. Genet.*, **38**, 191–196.
9. Valente, E.M., Logan, C.V., Mougou-Zerelli, S., Lee, J.H., Silhavy, J.L., Brancati, F., Iannicelli, M., Travaglini, L., Romani, S., Illi, B. *et al.* (2010) Mutations in TMEM216 perturb ciliogenesis and cause Joubert, Meckel and related syndromes. *Nat. Genet.*, **42**, 619–625.
10. Berbari, N.F., O'Connor, A.K., Haycraft, C.J. and Yoder, B.K. (2009) The primary cilium as a complex signaling center. *Curr. Biol.*, **19**, R526–R535.
11. Pazour, G.J. and Witman, G.B. (2003) The vertebrate primary cilium is a sensory organelle. *Curr. Opin. Cell Biol.*, **15**, 105–110.
12. Satir, P., Pedersen, L.B. and Christensen, S.T. (2010) The primary cilium at a glance. *J. Cell Sci.*, **123**, 499–503.
13. Goetz, S.C. and Anderson, K.V. (2010) The primary cilium: a signalling centre during vertebrate development. *Nat. Rev. Genet.*, **11**, 331–344.
14. Logan, C., Abdel-Hamed, Z. and Johnson, C. (2011) Molecular genetics and pathogenic mechanisms for the severe ciliopathies: insights into neurodevelopment and pathogenesis of neural tube defects. *Mol. Neurobiol.*, **43**, 12–26.
15. Lin, F., Hiesberger, T., Cordes, K., Sinclair, A.M., Goldstein, L.S.B., Somlo, S. and Igarashi, P. (2003) Kidney-specific inactivation of the KIF3A subunit of kinesin-II inhibits renal ciliogenesis and produces polycystic kidney disease. *Proc. Natl Acad. Sci. USA*, **100**, 5286–5291.
16. Cano, D.A., Murcia, N.S., Pazour, G.J. and Hebrok, M. (2004) orpk mouse model of polycystic kidney disease reveals essential role of primary cilia in pancreatic tissue organization. *Development*, **131**, 3457–3467.
17. Wilson, N.F. and Lefebvre, P.A. (2004) Regulation of flagellar assembly by glycogen synthase kinase 3 in Chlamydomonas reinhardtii. *Eukaryot. Cell*, **3**, 1307–1319.
18. Corbit, K.C., Shyer, A.E., Dowdle, W.E., Gaulden, J., Singla, V. and Reiter, J.F. (2008) Kif3a constrains [beta]-catenin-dependent Wnt signalling through dual ciliary and non-ciliary mechanisms. *Nat. Cell Biol.*, **10**, 70–76.
19. Lancaster, M.A., Schroth, J. and Gleeson, J.G. (2011) Subcellular spatial regulation of canonical Wnt signalling at the primary cilium. *Nat. Cell Biol.*, **13**, 700–707.
20. Huang, P. and Schier, A.F. (2009) Dampened Hedgehog signaling but normal Wnt signaling in zebrafish without cilia. *Development*, **136**, 3089–3098.
21. Ocbina, P.J.R., Tuson, M. and Anderson, K.V. (2009) Primary cilia are not required for normal canonical Wnt signaling in the mouse embryo. *PLoS ONE*, **4**, e6839.
22. Garcia-Gonzalo, F.R., Corbit, K.C., Sirerol-Piquer, M.S., Ramaswami, G., Otto, E.A., Noriega, T.R., Seol, A.D., Robinson, J.F., Bennett, C.L., Josifova, D.J. *et al.* (2011) A transition zone complex regulates mammalian ciliogenesis and ciliary membrane composition. *Nat. Genet.*, **43**, 776–784.
23. Xu, Y.K. and Nusse, R. (1998) The Frizzled CRD domain is conserved in diverse proteins including several receptor tyrosine kinases. *Curr. Biol.*, **8**, R405–R406.
24. Sergi, C., Kahl, P. and Otto, H.F. (2000) Contribution of apoptosis and apoptosis-related proteins to the malformation of the primitive intrahepatic biliary system in Meckel syndrome. *Am. J. Pathol.*, **156**, 1589–1598.
25. Lee, S.M., Tole, S., Grove, E. and McMahon, A.P. (2000) A local Wnt-3a signal is required for development of the mammalian hippocampus. *Development*, **127**, 457–467.
26. Galceran, J., Miyashita-Lin, E.M., Devaney, E., Rubenstein, J.L. and Grosschedl, R. (2000) Hippocampus development and generation of dentate gyrus granule cells is regulated by LEF1. *Development*, **127**, 469–482.
27. Mangale, V.S., Hirokawa, K.E., Satyaki, P.R.V., Gokulchandran, N., Chikbire, S., Subramanian, L., Shetty, A.S., Martynoga, B., Paul, J., Mai, M.V. *et al.* (2008) Lhx2 selector activity specifies cortical identity and suppresses hippocampal organizer fate. *Science*, **319**, 304–309.

28. Gulacsi, A.A. and Anderson, S.A. (2008) β-catenin-mediated Wnt signaling regulates neurogenesis in the ventral telencephalon. *Nat. Neurosci.*, **11**, 1383–1391.
29. Maria, B.L., Quisling, R.G., Rosainz, L.C., Yachnis, A.T., Gitten, J., Dede, D. and Fennell, E. (1999) Molar tooth sign in Joubert syndrome: clinical, radiologic, and pathologic significance. *J. Child Neurol.*, **14**, 368–376.
30. Corbit, K.C., Aanstad, P., Singla, V., Norman, A.R., Stainier, D.Y.R. and Reiter, J.F. (2005) Vertebrate Smoothened functions at the primary cilium. *Nature*, **437**, 1018–1021.
31. Tammachote, R., Hommerding, C.J., Sinders, R.M., Miller, C.A., Czarnecki, P.G., Leightner, A.C., Salisbury, J.L., Ward, C.J., Torres, V.E., Gattone, V.H. II *et al.* (2009) Ciliary and centrosomal defects associated with mutation and depletion of the Meckel syndrome genes MKS1 and MKS3. *Hum. Mol. Genet.*, **18**, 3311–3323.
32. Yanagawa, S., Lee, J.-S. and Ishimoto, A. (1998) Identification and characterization of a novel line of Drosophila Schneider S2 Cells that respond to Wingless signaling. *J. Biol. Chem.*, **273**, 32353–32359.
33. Lee, J.-S., Ishimoto, A. and Yanagawa, S.-I. (1999) Characterization of mouse Dishevelled (Dvl) proteins in Wnt/Wingless signaling pathway. *J. Biol. Chem.*, **274**, 21464–21470.
34. González-Sancho, J.M., Brennan, K.R., Castelo-Soccio, L.A. and Brown, A.M.C. (2004) Wnt proteins induce Dishevelled phosphorylation via an LRP5/6-independent mechanism, irrespective of their ability to stabilize β-Catenin. *Mol. Cell. Biol.*, **24**, 4757–4768.
35. Lancaster, M.A., Louie, C.M., Silhavy, J.L., Sintasath, L., DeCambre, M., Nigam, S.K., Willert, K. and Gleeson, J.G. (2009) Impaired Wnt-β-catenin signaling disrupts adult renal homeostasis and leads to cystic kidney ciliopathy. *Nat. Med.*, **15**, 1046–1054.
36. Park, T.J., Mitchell, B.J., Abitua, P.B., Kintner, C. and Wallingford, J.B. (2008) Dishevelled controls apical docking and planar polarization of basal bodies in ciliated epithelial cells. *Nat. Genet.*, **40**, 871–879.
37. Adams, M., Simms, R.J., Abdelhamed, Z., Dawe, H.R., Szymanska, K., Logan, C.V., Wheway, G., Pitt, E., Gull, K., Knowles, M.A. *et al.* (2012) A meckelin–filamin A interaction mediates ciliogenesis. *Hum. Mol. Genet.*, **21**, 1272–1286.
38. Khanna, H., Davis, E.E., Murga-Zamalloa, C.A., Estrada-Cuzcano, A., Lopez, I., den Hollander, A.I., Zonneveld, M.N., Othman, M.I., Waseem, N., Chakarova, C.F. *et al.* (2009) A common allele in RPGRIP1L is a modifier of retinal degeneration in ciliopathies. *Nat. Genet.*, **41**, 739–745.
39. Gattone, V.H., Tourkow, B.A., Trambaugh, C.M., Yu, A.C., Whelan, S., Phillips, C.L., Harris, P.C. and Peterson, R.G. (2004) Development of multiorgan pathology in the wpk rat model of polycystic kidney disease. *Anat. Rec. A Discov. Mol. Cell. Evol. Biol.*, **277A**, 384–395.
40. Cook, S.A., Collin, G.B., Bronson, R.T., Naggert, J.K., Liu, D.P., Akeson, E.C. and Davisson, M.T. (2009) A mouse model for Meckel syndrome type 3. *J. Am. Soc. Nephrol.*, **20**, 753–764.
41. Fraser, F.C., Lytwyn, A. and Opitz, J.M. (1981) Spectrum of anomalies in the Meckel syndrome, or: "Maybe there is a malformation syndrome with at least one constant anomaly". *Am. J. Med. Genet.*, **9**, 67–73.
42. Khaddour, R., Smith, U., Baala, L., Martinovic, J., Clavering, D., Shaffiq, R., Ozilou, C., Cullinane, A., Kyttälä, M., Shalev, S. *et al.* (2007) Spectrum of MKS1 and MKS3 mutations in Meckel syndrome: a genotype-phenotype correlation. *Hum. Mutat.*, **28**, 523–524.
43. Louie, C.M. and Gleeson, J.G. (2005) Genetic basis of Joubert syndrome and related disorders of cerebellar development. *Hum. Mol. Genet.*, **14**, R235–R242.
44. Gerdes, J.M., Liu, Y., Zaghloul, N.A., Leitch, C.C., Lawson, S.S., Kato, M., Beachy, P.A., Beales, P.L., DeMartino, G.N., Fisher, S. *et al.* (2007) Disruption of the basal body compromises proteasomal function and perturbs intracellular Wnt response. *Nat. Genet.*, **39**, 1350–1360.
45. Lancaster, M.A., Gopal, D.J., Kim, J., Saleem, S.N., Silhavy, J.L., Louie, C.M., Thacker, B.E., Williams, Y., Zaki, M.S. and Gleeson, J.G. (2011) Defective Wnt-dependent cerebellar midline fusion in a mouse model of Joubert syndrome. *Nat. Med.*, **17**, 726–731.
46. Huangfu, D., Liu, A., Rakeman, A.S., Murcia, N.S., Niswander, L. and Anderson, K.V. (2003) Hedgehog signalling in the mouse requires intraflagellar transport proteins. *Nature*, **426**, 83–87.
47. Huangfu, D. and Anderson, K.V. (2005) Cilia and Hedgehog responsiveness in the mouse. *Proc. Natl Acad. Sci. USA*, **102**, 11325–11330.
48. Liu, A., Wang, B. and Niswander, L.A. (2005) Mouse intraflagellar transport proteins regulate both the activator and repressor functions of Gli transcription factors. *Development*, **132**, 3103–3111.
49. Patterson, V.L., Damrau, C., Paudyal, A., Reeve, B., Grimes, D.T., Stewart, M.E., Williams, D.J., Siggers, P., Greenfield, A. and Murdoch, J.N. (2009) Mouse hitchhiker mutants have spina bifida, dorso-ventral patterning defects and polydactyly: identification of Tulp3 as a novel negative regulator of the Sonic hedgehog pathway. *Hum. Mol. Genet.*, **18**, 1719–1739.
50. Eggenschwiler, J.T., Bulgakov, O.V., Qin, J., Li, T. and Anderson, K.V. (2006) Mouse Rab23 regulates Hedgehog signaling from Smoothened to Gli proteins. *Develop. Biol.*, **290**, 1–12.
51. Norman, R.X., Ko, H.W., Huang, V., Eun, C.M., Abler, L.L., Zhang, Z., Sun, X. and Eggenschwiler, J.T. (2009) Tubby-like protein 3 (TULP3) regulates patterning in the mouse embryo through inhibition of Hedgehog signaling. *Hum. Mol. Genet.*, **18**, 1740–1754.
52. Bay, S.N. and Caspary, T. (2012) What are those cilia doing in the neural tube? *Cilia*, **1**, 19.
53. Burga, A., Casanueva, M.O. and Lehner, B. (2011) Predicting mutation outcome from early stochastic variation in genetic interaction partners. *Nature*, **480**, 250–253.
54. Queitsch, C., Sangster, T.A. and Lindquist, S. (2002) Hsp90 as a capacitor of phenotypic variation. *Nature*, **417**, 618–624.
55. Dawe, H.R., Smith, U.M., Cullinane, A.R., Gerrelli, D., Cox, P., Badano, J.L., Blair-Reid, S., Sriram, N., Katsanis, N., Attie-Bitach, T. *et al.* (2007) The Meckel-Gruber Syndrome proteins MKS1 and meckelin interact and are required for primary cilium formation. *Hum. Mol. Genet.*, **16**, 173–186.
56. Xu, J. (2005) Preparation, culture, and immortalization of mouse embryonic fibroblasts. *Curr. Protoc. Mol. Biol.*, Chapter 28:Unit 28.1.
57. Dawe, H.R., Adams, M., Wheway, G., Szymanska, K., Logan, C.V., Noegel, A.A., Gull, K. and Johnson, C.A. (2009) Nesprin-2 interacts with meckelin and mediates ciliogenesis via remodelling of the actin cytoskeleton. *J. Cell Sci.*, **122**, 2716–2726.
58. Willert, K., Brown, J.D., Danenberg, E., Duncan, A.W., Weissman, I.L., Reya, T., Yates, J.R. and Nusse, R. (2003) Wnt proteins are lipid-modified and can act as stem cell growth factors. *Nature*, **423**, 448–452.